Orientated growth of Copper-based MOF for acetylene storage

Zhanke Wang, Lei Ge, Mengran Li, Rijia Lin, Hao Wang, Zhonghua Zhu

PII: S1385-8947(18)31866-7
DOI: https://doi.org/10.1016/j.cej.2018.09.148
Reference: CEJ 19987

To appear in: *Chemical Engineering Journal*

Received Date: 11 May 2018
Revised Date: 6 September 2018
Accepted Date: 19 September 2018

Please cite this article as: Z. Wang, L. Ge, M. Li, R. Lin, H. Wang, Z. Zhu, Orientated growth of Copper-based MOF for acetylene storage, *Chemical Engineering Journal* (2018), doi: https://doi.org/10.1016/j.cej.2018.09.148

Orientated growth of Copper-based MOF for acetylene storage

Zhanke Wang,[a] Lei Ge,*[b] Mengran Li,[a] Rijia Lin,[a] Hao Wang [b] and Zhonghua Zhu *[a]

[a] School of Chemical Engineering, The University of Queensland, Brisbane 4072 Australia

[b] Center for Future Materials, University of Southern Queensland, Springfield Central, Queensland, 4300, Australia

Abstract

Manipulating crystal growth of metal-organic frameworks (MOF) has great potential in achieving unique properties for adsorption, separation and catalysis applications. For the first time, we used Mg/Al layered double hydroxide (LDH) nanosheets as modulators to tune the growth orientation of HKUST-1 without either pore blockage or crystallinity degradation. Through the introduction of LDH during hydrothermal process, HKUST-1 crystal shape transfers from octahedron with fully exposed {111} facets to tetrakaidecahedron with both {100} and {111} facets. The exposure of {100} facet with large pore size faciliates the activation of MOF, thereby providing more open metal sites. As a result, the micropore volume and BET surface area increase remarkably from 0.75 cm^3/g to 1.01 cm^3/g and 2255m^2/g to 3001 m^2/g, respectively. The tetrakaidecahedral HKUST-1 exhibits high acetylene uptake of 275 cm^3 (STP)/g at 298 K and 1 atm, which is the highest value ever reported to the best of our knowledge.

Keywords: Metal-organic frameworks, orientated growth, crystal shape, layered double hydroxide, acetylene adsorption

* *Corresponding author. Email: z.zhu@uq.edu.au (Z H Zhu) and l.ge@usq.edu.au (L Ge); Tel: +61 733653528, Fax: +61 733654199*

1. Introduction

Acetylene is an important feedstock for manufacturing many value-added chemical products and polymer materials in petrochemical and polyester industries.[1-3] However, acetylene storage is a daunting challenge because it becomes explosive when compressed to over 0.2Mpa at room temperature.[4, 5] For safety purposes, acetylene is usually stored in special cylinders filled with acetone and monolithic porous material, however this method suffers from low storage capacity, low gas withdrawal rate and no bulk storage.[2, 6] It is thus of great significant to develop economical and efficient porous materials with high acetylene storage.

Metal-organic frameworks (MOFs), consisting of inorganic metal centres coordinated with organic linkers, emerge recently as promising candidates for separation[7, 8], adsorption[9] and especially hydrocarbon storage[10-12] because of their exceptionally high microporosity, coordinatively unsaturated metal sites and uniformly structured cavities. Previous research on MOFs for acetylene storage mainly focused on designing new MOFs enriched with unsaturated metal sites and suitable micropores. For example, ZJU-12a with pore windows of 3.2 Å to 6.4 Å and unsaturated copper metals exhibited a remarkable high acetylene uptake capacity (244 cm^3/g at 298K and 1 atm).[11] Besides structure design of MOF by new pair of metal sources and organic ligands, orientated growth of MOFs with controllable pore geometry[13] and specific exposed facet[14] is an alternative strategy to improve the adsorption performance.

The crystal orientation of MOFs can be well controlled by epitaxial growth of MOFs on functionalised crystalline substrates. By using substrates with –COOH or –OH terminated self-assembled monolayers (SAMs), uniformly orientated three-dimensional MOFs (e.g. HKUST-1[13, 15], MOF-5[16]) can be grown epaxially in a layer-by-layer fashion, repeating immersing the substrate in a metal ion solution and a ligand molecules solution.[17] However, this method is very complex and time consuming, thereby not efficient and economical feasible for large-scale synthesis. Alternatively, chemical additives, such as surfactants, polymers and carboxylic acids

and their salts, have also been used as blocking agents, capping agents or modulators, showing high efficiency and repeatability for the orientated growth of MOFs.[14] For instance, lauric acid was used as the modulator to transform the HKUST-1 crystals from octahedron to tetrakaidecahedron and cube through accelerating the growth rate of <111> direction. However, these additives may induce crystallinity defects,[18] and are also difficult to be removed from MOFs micropore structures, thereby occupying the micropores and limiting the gas adsorption capacity. For example, adding cetyltrimethylammonium bromide (CTAB) during HKUST-1 synthesis facilitates the formation of nanocubes, but significantly reduced the specific surface area of the nanocubic product compared to the pristine HKUST-1.[18]

Herein, we developed a facile strategy to control the growth orientation of HKUST-1 without inducing pore block or crystallinity degradation, illustrated in Scheme 1. By using two-dimensional LDH nanosheets as modulator, the crystal shape of HKUST-1 could be changed from octahedron to tetrakaidecahedron and cube. After the shape manipulation, {100} facets are exposed gradually. The window size of {100} facets is 9 Å (for the purple pore cage) which is larger than that of {111} facets (4.6 Å, for the yellow sphere). That means, compared to octahedral HKUST-1fully exposed with {111} facets, the tetrakaidecahedral and cubic crystals can be activated more efficiently, leading to the enhancement of adsorption capacity by further increase of microporosity and surface area. By using this strategy, the as-obtained tetrakaidecahedral HKUST-1 exhibits superior acetylene uptake than reported MOFs and other porous materials. We hope this concept can pave a novel way to design MOFs materials for sufficient hydrocarbon storage.

2. Experimental

2.1 Materials

All chemicals including magnesium chloride hexahydrate ($MgCl_2$•$6H_2O$, 99%), aluminium chloride hexahydrate ($AlCl_3$•$6H_2O$, 99%), sodium hydroxide (NaOH, 98%) and sodium carbonate (Na_2CO_3, 99%), copper (II) nitrate trihydrate ($Cu(NO_3)_2$•$3H_2O$, 99%), 1,3,5-benzene tricarboxylic acid (H_3BTC, 95%), N,N-dimethylformamide (DMF, 99.5%), were purchased from Sigma-Aldrich without further purification. AR grade ethanol and methanol were obtained from Merck.

2.2 Synthesis of Mg/Al-LDH

Mg/Al-LDH nanosheets were prepared based on a reference[19] with some modifications. 10ml salt solution containing 0.2M magnesium chloride hexahydrate and 0.1M aluminium chloride hexahydrate were added into 40ml mixed basic solution containing 0.15M sodium hydroxide and 0.013M sodium carbonate under vigorously stirring for 30 minutes. The obtained LDH was washed by centrifuging and redispersing in deionized water for twice. Redispersing the LDH precursor in 45 mL of deionized water, the slurry was then transferred into a steel autoclave to heat at 100 °C for 16 hours. The obtained LDH (0.4 g) was re-dispersed in 15 mL of deionized water for the use in HKUST-1 synthesis.

2.3 Synthesis of orientated HKUST-1

HKUST-1 was prepared by solvothermal synthesis similar to previous work.[20] About 0.335 g H_3BTC was dissolved in 10 ml of a 1: 1 mixture of ethanol and N,N-dimethylformamide. In another beaker, 0.692 g copper (II) nitrate trihydrate were dissolved in 5 mL water. For controlling crystal growth orientation, different amount of above LDH slurry (0, 2.8 and 4.7 mL) were mixed with metal precursor solution under sonication. Then metal solution and organic ligand solution were mixed and stirred for 15 minutes before transferring into a Teflon-lined stainless steel autoclave. After hydrothermal reaction at 100 °C for 7 h, blue crystals were obtained and then washed by DMF and methanol for 6 times. During each washing process, ultrasonic was utilised at the first 10min and then the supernatant solvents with small crystal were

replaced with fresh methanol for another two hours.. The final supernatant solvents should be clear and the blue products were dried in a vacuum oven at room temperature for 2 h and then 60 °C for 8h.

Time-dependent experiments were carried out as normal procedure. The difference was that after heating for certain time the autoclave were cooled to room temperature in 5 minutes and then the as-prepared crystals were separated immediately by centrifugation. After washed with methanol for twice, all products were collected by centrifugation.

2.4 Characterization

The X-ray diffraction spectra (XRD) of as-obtained HKUST-1 crystals were obtained with a Bruker Advanced X-Ray Diffractometer (40 kV, 30 mA) with Cu Kα (λ=0.15406 nm) radiation at a scanning rate of 1^o/min from 5^o to 50^o. Electron microscope images of synthesised samples were collected on a JEOL JSM-7001F scanning electron microscopy with X-ray energy dispersive analysis spectroscopy (EDS) and a JEOL JEM2100 LaB_6 S transmission electron microscopy operated at 200 kV. Thermogravimetric analysis was carried out using a Perkin Elmer Instruments STA 6000 Thermo Gravimetric Analyser with a heating rate of 5 °C form 30 to 800 °C under air. Inductively Coupled Optical Emission Spectrometer (ICP-OES) analysis was performed using a Perkin Elmer Optima 8300 DV.

Gas sorption isotherms were performed on a Micromeritics TriStar II 3020 and samples were degassed at 150 °C for 12 h. The N_2 sorption measurement was maintained at 77 K. The C_2H_2, CO_2 and C_2H_6 sorption measurements were performed at 273 K with an ice-water bath and at 298 K with a water bath. Total specific surface areas were determined by the BET method using relative pressure of 0.01-0.05. Micropore volumes were obtained by both t-plot (N_2, 77K) and Dubin method (CO_2, 273K). Pore size distribution was determined by density functional theory (DFT) method using CO_2 adsorption isotherm at 273K.

3. Results and discussions

3.1 Synthesis of HKUST-1 with different morphologies

Figure 1 shows the morphology of HKUST-1 crystals obtained by adding different amount of Mg/Al-LDH (LDH/BTC molar ratio=0, 0.03 and 0.05) during solvethermal synthesis. The samples synthesized without the addition of LDH (refer to Mg/Al-LDH) are typical octahedron and the mean size of particle is about 12 μm (Figure 1a and S1a). When LDH slurry was added (LDH/BTC molar ratio=0.03), tetrakaidecahedral (Figure 1b and S1b) crystals with average size of 9 μm can be obtained. Cubic crystals (Figure 1c and S1c) with average 6 μm particle size can be achieved with further increment of LDH addition (LDH/BTC molar ratio=0.05). Obviously, the shape of as-prepared products transferred from octahedron to tetrakaidecahedron and cube with reduced crystals size (Figure S1).

To identify the crystalline structures of the samples, powder X-ray diffraction measurement was performed. Figure 2 presents the corresponding XRD patterns of octahedral, tetrakaidecahedral and cubic samples. It is clearly that all the characteristic diffraction peaks of crystal products match well with the simulated peaks of HKUST-1. And the relative peak intensities of 6.75^{o}, 9.51^{o} and 13.47^{o} of cubic HKUST-1, assigning to the (200), (220) and (400) lattices, respectively, significantly increase as compared to those of octahedral HKUST-1, indicating a preferential crystal growth of HKUST-1 along the <100> direction. In addition, no characteristic reflections for impurity phases were detectable in XRD pattern. Meanwhile, no Mg and Al signal can be observed in localised EDS scan of HKUST-1 crystal synthesised by LDH modulation (Figure S3), indicating the obtain of high purity HKUST-1. ICP-OES was further applied to analyse the potential existence of impurity in modulated HKUST-1. As shown in Table S1, trace amounts of Mg (0.003~0.01 wt%) and small amounts of Al (0.16~0.36 wt%) was detected among the tetrakaidecahedral and cubic HKUST-1 and their residual concentrations increased with LDH

modulation content. As a conclusion, only negligible LDH was incorporated into the HKUST-1 products during the modulation, while small amount of Al containing impurities can be formed at high LDH modulation condition.

3.2 Growth mechanism of various morphologies of HKUST-1

In order to gain an insight into the evolution process of HKUST-1 morphologies, a series of time-dependent solvothermal experiments was carried out and the process of crystal growth was monitored by SEM and XRD (Figure 3). It is noteworthy that negligible amount of crystals were obtained before solvethermal process at the absent of LDH. However, large amount of crystals could be obtained after 15min stirring when LDHs were added. This phenomenon is attributed to the hydroxyl groups on the surface of LDH that can deprotonate the H_3BTC ligand. As a result, the crystal-growth units were rapidly yielded and much more crystal were obtained compared to the case without LDH. [21] As shown in Figure 3a-c, octahedral crystals grew gradually alone <111> direction at the absence of LDH. When medium amount (LDH/BTC =0.03) of LDH was employed, the evolution from octahedron to tetrakaidecahedron (Figure 3e-g) and preferential growth alone <100> (Figure 3h) were observed during crystal growth. Further increase of LDH (LDH/BTC =0.05) resulted in the formation of tetrakaidecahedral crystals even before the solvothermal reaction (Figure 3i). This result could be explained by surface-energy-driven mechanism.[21] The surface energy of {111} facets is lower than the {100} surface. Octahedral crystals with 8 {111} facets are the most stable structure and could be formed without any additives. With the addition of LDH, supersaturation of HKUST-1 crystal-growth units increased significantly, resulting the appearance of tetrakaidecahedral HKUST-1 with high-energy surfaces {100}. During the solvethermal process, the surface {100} facets of the tetrakaidecahedral HKUST-1 became larger, therefore the shape transformation to cubic crystals occurs at 60min

solvothermal reaction (Figure 3k). The orientated growth alone <100> can also be observed from the increase of relative intensity of (200) and (400) in Figure 3l.

To probe the intrinsic factors governing the orientated growth of HKUST-1, the time-dependent concentrations of Cu, Al and Mg ion in reaction solution of HKUST-1 (LDH/BTC =0.03) were measured. As shown in Figure S5, the concentration of Al and Mg ions increased gradually by leaching LDH. Then the Al ions concentration decreased gradually after the appearance of tetrakaidecahedral HKUST-1 (~45 min), while the Mg ions concentration remained at same level. This phenomenon indicates that the Al ions play an important role on the preferential growth of HKUST-1. To further investigate the crystal growth mechanism, the comparison experiments was conducted subsequently by directly adding aluminium nitrate into the precursor solution instead of LDH. As presented in Figure S6, octahedral crystals began to appear after 30min solvothermal reaction, while the nucleation of HKUST-1 synthesized without Al ions was occurred in short time (<15min) . This implied that the coordination of Cu ions and BTC ligands was suppressed because of the competing reaction of Al ions and BTC ligands. With prolonging the reaction time, tetrakaidecahedral (Figure S6b), truncated cubic (Figure S6c) and cubic (Figure S6d) crystals were obtained. Notably, many rod-like micron-sized impurities can be observed in the final products. The EDS in Figure S3e displays that there is Al signal in those rods, implying that the impurities was formed because of the reaction of Al ions and BTC ligands. The morphology evolution could be explained by the BFDH (Bravais, Friedel, Donnay and Harker) law.[22] According to the law, different facets of crystal have different growth rate and the slowest growth facet dominates the shape of crystal. The growth rate of a facet is inversely proportional to the lattice spacing, dhkl.[23] As to HKUST-1, {111} face with largest d-spacing (15.1723Å) has lowest growth rate, resulting in the formation of octahedral crystals with 8 {111} facets at the absence of additives. When Al ions were involved, it could compete with Cu ions to link with

BTC ligands, which constrained the growth rate of {100} facets profoundly. Therefore, when the growth rate of {100} facets and {111} facets were very close ($\nu_{\{100\}} \approx \nu_{\{111\}}$), tetrakaidecahedral HKUST-1 will be obtained. When increasing the amount of LDH, more Al ions could be released and $\nu_{\{100\}}$ became much smaller than $\nu_{\{111\}}$, leading to the formation of cubic HKUST-1.

The potential mechanism of orientated HKUST-1 growth by LDH modulation is illustrated in Scheme 2. Overall, there are two stages in the formation of HKUST-1: nucleation and crystal growth. In the first stage, the addition of LDH could accelerate the deprotonation of H_3BTC, resulting in high supersaturation and fast nucleation rate. Thus the formation of tetrakaidecahedral crystal with {100} facets can be facilitated at early stage. In the second stage, the preferential growth of {100} facets was induced by the competitive reaction between Al ions and Cu ions with BTC ligands, resulting in the shape evolution.

3.3 Stability, surface area and pore volume analysis

Thermal and chemical stability of the materials is essential for industrial application.[24, 25] The TGA curves of serials of HKUST-1 crystals are presented in Figure 4a. Similar to referenced HKUST-1[26, 27], all samples with different shapes are thermally stable up to 250 °C and have a similar sharp weight loss attributed to decomposition of BTC (280 ~330 °C). To investigate the chemical stability, as-prepared three samples were immersed in harsh condition (pH=3 HNO_3 solution and pH=11 NaOH) for 24h at room temperature and the change of crystal structure was characterized by XRD. As shown in Figure 4, all those three samples could retain their original phase structures in pH=3 HNO_3 solutions. However, when they were exposed in pH= 11 NaOH solution, the octahedron suffered more destruction than the cube. This indicated that the exposure of {100} facets could promote the tolerance towards alkaline media.

The surface area and microporosity of MOF materials are crucial for the gas adsorption. Figure 5 shows typical type I isotherms of N_2 adsorption for all three HKUST-1 samples. The high N_2

adsorption capacity at low relative pressure indicates that all HKUST-1 samples are micropore dominant. As shown in Table 1, the octahedral HKUST-1 has a BET surface area of 2255 m^2/g consistent with reported values.[4, 28] The oriented growth of HKUST-1 by LDH modulation increased the surface area significantly. The tetrakaidecahedral HKUST-1 exhibited a surface area of ~3000 m^2/g, which was much higher than HKUST-1 obtained from different synthesis and activation conditions.[29, 30] The surface area of cubic HKUST-1 is larger than the octahedron but smaller than the tetrakaidecahedron. As compared with other methods for achieving the orientated growth of HKUST-1,[18] the higher surface area and microporosity achieved in this study indicates the minimisation of pore blockage and crystal defects. The enhancement of HKUST-1 surface area by preferential growth could be attributed to the sufficient remove of DMF during solvent activation. As shown in Figure S7, the presence of N elements of octahedral HKUST-1 was confirmed by N 1s peak. While tetrakaidecahedral and cubic HKUST-1 with {100} facets showed no obviously N signal. This phenomenon could be explained as follow. As a kind of face-centred cubic (fcc, space group $Fm\bar{3}m$) structure, the structure unit of HKUST-1 has two types of facets (shown in Figure 6): a small triangle window size of 0.46 nm for <111> orientation and a large square one of 0.9 nm for <100> orientation.[14] The kinetic diameter of DMF is about 0.55 nm which is larger than the window size of {111} facets and smaller than that of {100}. Therefore, the exposure of {100} facets could facilitate the remove of DMF during activation, leading to higher BET surface area of the tetrakaidecahedral and cubic HKUST-1 than that of octahedral HKUST-1. The observed BET surface area of cubic HKUST-1 was slightly lower than that of tetrakaidecahedral one, it is probably due to that the Al-BTC impurities derived from high LDH addition cannot be fully washed out.

Both surface area and micropore volume play significant roles in the adsorption capacity of micro materials. The calculated micropore volumes of HKUST-1 samples are summarised in Table

1.The referenced octahedral HKUST-1 has a micropore volume of 0.748 cm^3/g, which is in the range of the values reported in the literatures.[28, 31, 32] The tetrakaidecahedral crystals have much higher micropore volume (1.011 cm^3/g) than the octahedral and cubic ones. In order to understand the pore geometry difference, pore size distributions of those HKUST-1 were depicted in Figure S8. Compared with octahedral HKUST-1, the tetrakaidecahedral and cubic one has more large pores (around 0.9 nm) as a result of the fully exposed {100} facets. Overall, the exposed large pore windows in tetrakaidecahedral and cubic HKUST-1 will benefit the activation and provide more accessible micropores for gas uptake, expecting better adsorption capacity than octahedral HKUST-1.

3.4 Gas adsorption measurement

Gas-adsorption measurements for as-prepared HKUST-1 were carried out using C_2H_2, CO_2 and C_2H_6. All gas-adsorption isotherms were measured after pre-treatment under a dynamic vacuum at 150 ^oC. The low-pressure acetylene adsorption of different shaped HKUST-1 was evaluated at both 273K and 298K. As shown in Figure 7a, the C_2H_2 uptake of tetrakaidecahedral HKUST-1(409 cm^3 (STP)/g) is much higher than that of the octahedral (305 cm^3 (STP)/g) and cubic ones (352 cm^3 (STP)/g) at 273K, 1 atm. C_2H_2 uptake at room temperature (298K) were also studied considering the practical storage condition(Figure 7b). The tetrakaidecahedral HKUST-1 still has the extraordinary C_2H_2 uptake (275 cm^3 (STP)/g) at 298K, which is higher than all the reported acetylene storage materials, summarised in Table 2. The cubic one also exhibits favourable C_2H_2 uptake at 239 cm^3 (STP)/g, while that of octahedron reaches 223 cm^3 (STP)/g. There are two strong binding sites (open metal sites and small side pockets) and a weak binding site (large cage) for the adsorption of C_2H_2 on HKUST-1.[33] For the octahedral HKUST-1, residual DMF could occupy some open metal sites, resulting in lower C_2H_2 uptake than that of tetrakaidecahedral and cubic HKUST-1. As to the cubic HKUST-1, the existence of impurities in cubic HKUST-1 limits

the further increase of C_2H_2 uptake capability. CO_2 adsorption isotherm in Figure S9a was quite similar with that of C_2H_2 (Figure 7a). This could be easily understood by the fact that both CO_2 and C_2H_2 are liner molecule and their kinetic diameter are 0.33 nm.[34] Nevertheless, the C_2H_6 adsorption isotherm on HKUST-1 with different shapes are quite different (Figure S9b). The C_2H_6 adsorbed more on the tetrakaidecahedron than the others at low pressure. This may be attributed to the steric hindrance effect of larger C_2H_6 molecules (0.44nm) and the impurities in cubic HKUST-1. The gas-adsorption measurement shows that the tetrakaidecahedral HKUST-1 is a potential candidate for gas storage and adsorption.

4. Conclusions

In summary, using LDH as modulator can be a facile and effective method for orientated growth of HKUST-1. With increasing LDH concentration, crystal shape transfers from octahedron to tetrakaidecahedron and cube. Tetrakaidecahedral HKUST-1 with both {100} and {111} facets exhibited higher surface area (3001 m^2/g) and micropore volume (1.011 cm^3/g) than the other two shapes of HKUST-1. The ultrahigh C_2H_2 uptake of 275 cm^3 (STP)/g was also observed on tetrakaidecahedral HKUST-1 at 298K under atmospheric pressure, indicating the practical potential for acetylene storage. The possible role of LDH in orientated growth mechanism was investigated. The methodology for oriented growth of MOFs presented in this study will provide useful insights in fine-tuning microstructure of MOFs for various applications, such as adsorption, catalysis and sensing.

Supporting Information

SEM morphologies of obtained HKUST-1 from different LDH/BTC molar ratio, XRD patterns, SEM, HRTEM and SAED images of Mg/Al-LDH, EDS patterns of oriented HKUST-1, SEM

images of HKUST-1 synthesized by adding Al ions, XPS survey spectrums of oriented HKUST-1 pore size distributions of oriented HKUST-1.

Acknowledgements

Z. Zhu wants to thank the financial support by ARC Future Fellowship FT120100720. Z. Wang acknowledges financial support from China Scholarship Council. The authors also acknowledge the scientific and technical assistance of the Australian Microscopy and Microanalysis Research Facility at the UQ Centre. The authors thank David Appleton and Anya Yago for their kind help on the ICP and XRD characterization.

References

[1] R. Matsuda, R. Kitaura, S. Kitagawa, Y. Kubota, R.V. Belosludov, T.C. Kobayashi, H. Sakamoto, T. Chiba, M. Takata, Y. Kawazoe, Y. Mita, Highly controlled acetylene accommodation in a metal-organic microporous material, Nature 436 (2005) 238-241.

[2] T.L. Hu, H. Wang, B. Li, R. Krishna, H. Wu, W. Zhou, Y. Zhao, Y. Han, X. Wang, W. Zhu, Z. Yao, S. Xiang, B. Chen, Microporous metal-organic framework with dual functionalities for highly efficient removal of acetylene from ethylene/acetylene mixtures, Nat. Commun. 6 (2015) 7328-7336.

[3] Z. Zhang, S. Xiang, B. Chen, Microporous metal–organic frameworks for acetylene storage and separation, CrystEngComm 13 (2011) 5983-5992.

[4] S.C. Xiang, W. Zhou, J.M. Gallegos, Y. Liu, B.L. Chen, Exceptionally High Acetylene Uptake in a Microporous Metal-Organic Framework with Open Metal Sites, J. Am. Chem. Soc. 131 (2009) 12415-12419.

[5] M. Zhang, B. Li, Y. Li, Q. Wang, W. Zhang, B. Chen, S. Li, Y. Pan, X. You, J. Bai, Finely tuning MOFs towards high performance in C_2H_2 storage: synthesis and properties of a new

MOF-505 analogue with an inserted amide functional group, Chem. Commun. 52 (2016) 7241-7244.

[6] J. Pang, F. Jiang, M. Wu, C. Liu, K. Su, W. Lu, D. Yuan, M. Hong, A porous metal-organic framework with ultrahigh acetylene uptake capacity under ambient conditions, Nat. Commun. 6 (2015) 7575-7581.

[7] C.B. Fan, L. Le Gong, L. Huang, F. Luo, R. Krishna, X.F. Yi, A.M. Zheng, L. Zhang, S.Z. Pu, X.F. Feng, M.B. Luo, G.C. Guo, Significant Enhancement of C_2H_2/C_2H_4 Separation by a Photochromic Diarylethene Unit: A Temperature- and Light-Responsive Separation Switch, Angew. Chem. Int. Ed. 56 (2017) 7900-7906.

[8] F. Luo, C. Yan, L. Dang, R. Krishna, W. Zhou, H. Wu, X. Dong, Y. Han, T.L. Hu, M. O'Keeffe, L. Wang, M. Luo, R.B. Lin, B. Chen, UTSA-74: A MOF-74 Isomer with Two Accessible Binding Sites per Metal Center for Highly Selective Gas Separation, J. Am. Chem. Soc. 138 (2016) 5678-5684.

[9] M.B. Luo, Y.Y. Xiong, H.Q. Wu, X.F. Feng, J.Q. Li, F. Luo, The MOF^+ Technique: A Significant Synergic Effect Enables High Performance Chromate Removal, Angew. Chem. Int. Ed. 56 (2017) 16376-16379.

[10] K. Liu, D. Ma, B. Li, Y. Li, K. Yao, Z. Zhang, Y. Han, Z. Shi, High storage capacity and separation selectivity for C2 hydrocarbons over methane in the metal–organic framework Cu–TDPAT, J. Mater. Chem. A 2 (2014) 15823-15828.

[11] X. Duan, Y. Cui, Y. Yang, G. Qian, A novel methoxy-decorated metal–organic framework exhibiting high acetylene and carbon dioxide storage capacities, CrystEngComm 19 (2017) 1464-1469.

[12] X. Rao, J. Cai, J. Yu, Y. He, C. Wu, W. Zhou, T. Yildirim, B. Chen, G. Qian, A microporous metal-organic framework with both open metal and Lewis basic pyridyl sites for high C_2H_2 and CH4 storage at room temperature, Chem. Commun. 49 (2013) 6719-6721.

[13] E. Biemmi, C. Scherb, T. Bein, Oriented growth of the metal organic framework $Cu_3(BTC)_2(H_2O)_3 \cdot xH_2O$ tunable with functionalized self-assembled monolayers, J. Am. Chem. Soc. 129 (2007) 8054-8055.

[14] Y. Mao, B. Su, W. Cao, J. Li, Y. Ying, W. Ying, Y. Hou, L. Sun, X. Peng, Specific oriented metal-organic framework membranes and their facet-tuned separation performance, ACS Appl. Mater. Interfaces 6 (2014) 15676-15685.

[15] O. Shekhah, H. Wang, S. Kowarik, F. Schreiber, M. Paulus, M. Tolan, C. Sternemann, F. Evers, D. Zacher, R.A. Fischer, C. Woll, Step-by-step route for the synthesis of metal-organic frameworks, J. Am. Chem. Soc. 129 (2007) 15118-15119.

[16] S. Hermes, F. Schroder, R. Chelmowski, C. Woll, R.A. Fischer, Selective nucleation and growth of metal-organic open framework thin films on patterned COOH/CF_3-terminated self-assembled monolayers on Au(111), J. Am. Chem. Soc. 127 (2005) 13744-13745.

[17] H. Gliemann, C. Wöll, Epitaxially grown metal-organic frameworks, Mater. Today 15 (2012) 110-116.

[18] Q. Liu, L.N. Jin, W.Y. Sun, Facile fabrication and adsorption property of a nano/microporous coordination polymer with controllable size and morphology, Chem. Commun. 48 (2012) 8814-8816.

[19] Z. Xu, G. Stevenson, C. Lu, G. Lu, Dispersion and size control of layered double hydroxide nanoparticles in aqueous solutions, J. Phys. Chem. B 110 (2006) 16923-16929.

[20] Y. Yang, P. Shukla, S. Wang, V. Rudolph, X.-M. Chen, Z. Zhu, Significant improvement of surface area and CO_2 adsorption of Cu–BTC via solvent exchange activation, RSC Adv. 3 (2013) 17065-17072.

[21] Q. Liu, J.M. Yang, L.N. Jin, W.Y. Sun, Controlled synthesis of porous coordination-polymer microcrystals with definite morphologies and sizes under mild conditions, Chem. Eur. J. 20 (2014) 14783-14789.

[22] D. Li, H. Wang, X. Zhang, H. Sun, X. Dai, Y. Yang, L. Ran, X. Li, X. Ma, D. Gao, Morphology Design of IRMOF-3 Crystal by Coordination Modulation, Cryst. Growth Des. 14 (2014) 5856-5864.

[23] A. Umemura, S. Diring, S. Furukawa, H. Uehara, T. Tsuruoka, S. Kitagawa, Morphology design of porous coordination polymer crystals by coordination modulation, J. Am. Chem. Soc. 133 (2011) 15506-15513.

[24] Y.Y. Jia, X.T. Liu, W.H. Wang, L.Z. Zhang, Y.H. Zhang, X.H. Bu, A Sr^{2+}-metal-organic framework with high chemical stability: synthesis, crystal structure and photoluminescence property, Phil. Trans. R. Soc. A 375 (2017).

[25] X. Chen, H. Jiang, B. Hou, W. Gong, Y. Liu, Y. Cui, Boosting chemical stability, catalytic activity, and enantioselectivity of metal-organic frameworks for batch and flow reactions, J. Am. Chem. Soc. 139 (2017) 13476-13482.

[26] R. Zhang, L. Hu, S. Bao, R. Li, L. Gao, R. Li, Q. Chen, Surface polarization enhancement: high catalytic performance of Cu/CuOx/C nanocomposites derived from Cu-BTC for CO oxidation, J. Mater. Chem. A 4 (2016) 8412-8420.

[27] Y. Wang, Y. Lü, W. Zhan, Z. Xie, Q. Kuang, L. Zheng, Synthesis of porous Cu_2O/CuO cages using Cu-based metal–organic frameworks as templates and their gas-sensing properties, J. Mater. Chem. A 3 (2015) 12796-12803.

[28] J.A. Mason, M. Veenstra, J.R. Long, Evaluating metal–organic frameworks for natural gas storage, Chem. Sci. 5 (2014) 32-51.

[29] S. Liu, L. Sun, F. Xu, J. Zhang, C. Jiao, F. Li, Z. Li, S. Wang, Z. Wang, X. Jiang, H. Zhou, L. Yang, C. Schick, Nanosized Cu-MOFs induced by graphene oxide and enhanced gas storage capacity, Energ. Environ. Sci. 6 (2013) 818-823.

[30] Y. Mao, L. Shi, H. Huang, W. Cao, J. Li, L. Sun, X. Jin, X. Peng, Room temperature synthesis of free-standing HKUST-1 membranes from copper hydroxide nanostrands for gas separation, Chem. Commun. 49 (2013) 5666-5668.

[31] Y. Peng, V. Krungleviciute, I. Eryazici, J.T. Hupp, O.K. Farha, T. Yildirim, Methane storage in metal-organic frameworks: current records, surprise findings, and challenges, J. Am. Chem. Soc. 135 (2013) 11887-11894.

[32] P. Chowdhury, S. Mekala, F. Dreisbach, S. Gumma, Adsorption of CO, CO_2 and CH_4 on Cu-BTC and MIL-101 metal organic frameworks: Effect of open metal sites and adsorbate polarity, Microporous Mesoporous Mater. 152 (2012) 246-252.

[33] V.K. Peterson, Y. Liu, C.M. Brown, C.J. Kepert, Neutron powder diffraction study of D2 sorption in Cu_3(1, 3, 5-benzenetricarboxylate)$_2$, J. Am. Chem. Soc. 128 (2006) 15578-15579.

[34] R. Eguchi, S. Uchida, N. Mizuno, Inverse and high CO_2/C_2H_2 sorption selectivity in flexible organic-inorganic ionic crystals, Angew. Chem. Int. Ed. Engl. 51 (2012) 1635-1639.

[35] F. Moreau, I. da Silva, N.H. Al Smail, T.L. Easun, M. Savage, H.G. Godfrey, S.F. Parker, P. Manuel, S. Yang, M. Schroder, Unravelling exceptional acetylene and carbon dioxide adsorption within a tetra-amide functionalized metal-organic framework, Nat. Commun. 8 (2017) 14085-14084.

[36] H.M. Wen, H. Wang, B. Li, Y. Cui, H. Wang, G. Qian, B. Chen, A Microporous Metal-Organic Framework with Lewis Basic Nitrogen Sites for High C_2H_2 Storage and

Significantly Enhanced C_2H_2/CO_2 Separation at Ambient Conditions, Inorg. Chem. 55 (2016) 7214-7218.

[37] C. Song, J. Jiao, Q. Lin, H. Liu, Y. He, C_2H_2 adsorption in three isostructural metal-organic frameworks: boosting C_2H_2 uptake by rational arrangement of nitrogen sites, Dalton Trans. 45 (2016) 4563-4569.

[38] J. Jiao, L. Dou, H. Liu, F. Chen, D. Bai, Y. Feng, S. Xiong, D.-L. Chen, Y. He, An aminopyrimidine-functionalized cage-based metal–organic framework exhibiting highly selective adsorption of C_2H_2 and CO_2 over CH_4, Dalton Trans. 45 (2016) 13373-13382.

[39] T. Xia, J. Cai, H. Wang, X. Duan, Y. Cui, Y. Yang, G. Qian, Microporous metal-organic frameworks with suitable pore spaces for acetylene storage and purification, Microporous Mesoporous Mater. 215 (2015) 109-115.

[40] S. Xiang, W. Zhou, Z. Zhang, M.A. Green, Y. Liu, B. Chen, Open metal sites within isostructural metal–organic frameworks for differential recognition of acetylene and extraordinarily high acetylene storage capacity at room temperature, Angew. Chem. Int. Ed. 49 (2010) 4615-4618.

[41] X. Duan, C. Wu, S. Xiang, W. Zhou, T. Yildirim, Y. Cui, Y. Yang, B. Chen, G. Qian, Novel microporous metal-organic framework exhibiting high acetylene and methane storage capacities, Inorg. Chem. 54 (2015) 4377-4381.

[42] S. Yang, A.J. Ramirez-Cuesta, R. Newby, V. Garcia-Sakai, P. Manuel, S.K. Callear, S.I. Campbell, C.C. Tang, M. Schroder, Supramolecular binding and separation of hydrocarbons within a functionalized porous metal-organic framework, Nat. Chem. 7 (2014) 121-129.

[43] H. Wang, B. Li, H. Wu, T.L. Hu, Z. Yao, W. Zhou, S. Xiang, B. Chen, A Flexible Microporous Hydrogen-Bonded Organic Framework for Gas Sorption and Separation, J. Am. Chem. Soc. 137 (2015) 9963-9970.

FIGURE CAPTIONS:

Scheme 1. Schematic illustrations of the orientated growth of (a) octahedral, (b) tetrakaidecahedral and (c) cubic HKUST-1 crystal by LDH modulation.

Scheme 2. Schematic illustrations of the mechanism for the orientated growth of HKUST-1 by LDH modulation.

Figure 1. SEM images of octahedral (a), tetrakaidecahedral (b) and cubic (c) HKUST-1 prepared with different LDH/BTC molar ratio (a: 0; b: 0.03; c: 0.05)

Figure 2. XRD patterns of as-prepared octahedral (a), tetrakaidecahedral (b), cubic (c) and simulated HKUST-1

Figure 3. Morphological evolution of octahedral (a, b, c, d), tetrakaidecahedral (e, f, g, h), cubic (i, g, k, l) HKUST-1 synthesised with different heating duration time of 0 (a, e, i), 30 (b), 45(f), 60 (j, c), 75 (g) and 120min (k); Corresponding XRD pattern were shown at the bottle of SEM image.

Figure 4. TGA curves of HKUST-1 (a) and XRD patterns of octahedral (b), tetrakaidecahedral (c), cubic (d) HKUST-1 under different conditions.

Figure 5. N_2 sorption isotherms at 77K for HKUST-1 with different morphologies

Figure 6. Unit cells of HKUST-1 projected along <111> (a) and <100> (c); (b) a standard growth unit with 8 triangle window (yellow) for {111} facets and 6 square window (purple) for {100} facets

Figure 7. Acetylene adsorption isotherms of HKUST-1 with different morphologies at 273K (a) and 298K (b)

Table 1. Surface area and micropore volume of HKUST-1 with different morphologies

HKUST-1	BET special surface area [m^2/g]	T-plot Micropore area[m^2/g]	DUBIN Micropore volume [cm^3/g]	T-plot Micropore volume [cm^3/g]
octahedron	2255	1917	1.115	0.748
tetrakaidecahedron	3001	2580	1.482	1.011
cube	2642	2279	1.251	0.890

Table 2 Comparison of BET surface area, pore volume and C_2H_2 uptake in reported porous materials at 298K and 1 atm

MOFs	Surface area (BET) (m^2/g)	pore volume (cm^3/g)	C_2H_2 uptake STP (cm^3/g)	C_2H_2 uptake STP (cm^3/cm^3)	Ref.
HKUST-1 tetrakaidecahedron	3001	1.01	275	242	This work
HKUST-1 cube	2642	0.89	239	210	This work
ZJU-12a	2316	0.94	244	195	[11]
MFM-188	2568	-	232	193	[35]
FJI-H8	2025	0.82	224	196	[6]
NJU-Bai-17	2423	0.91	222.4	187	[5]

ZJU-40a	2858	1.06	216	237	[36]
ZJNU-47	2638	1.03	213	157	[37]
ZJNU-54	2134	0.87	211	171	[38]
Cu_2TPTC-Ome	2278	1.04	204	163	[39]
HKUST-1	2095	0.76	201	177	[4]
CoMOF-74	1504	0.63	197	230	[40]
ZJU-70a	1791	0.68	191	167	[41]
NOTT-300	1370	0.43	142	189	[42]
HOF-5a	1101	0.55	102	97	[43]

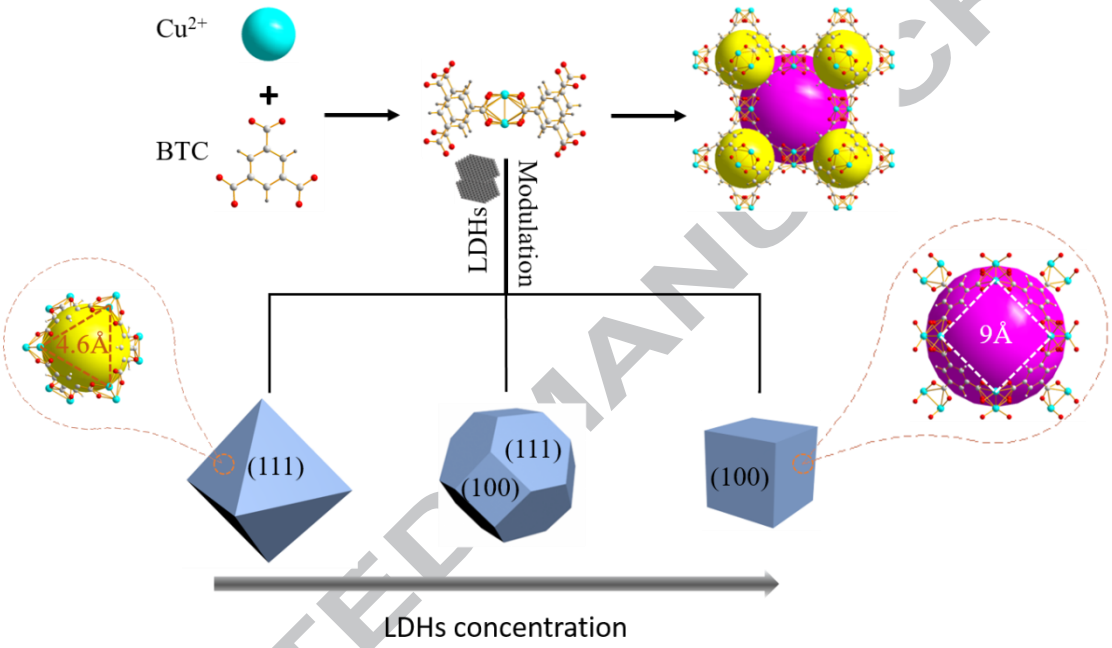

Scheme 1. Schematic illustrations of the orientated growth of (a) octahedral, (b) tetrakaidecahedral and (c) cubic HKUST-1 crystal by LDH modulation.

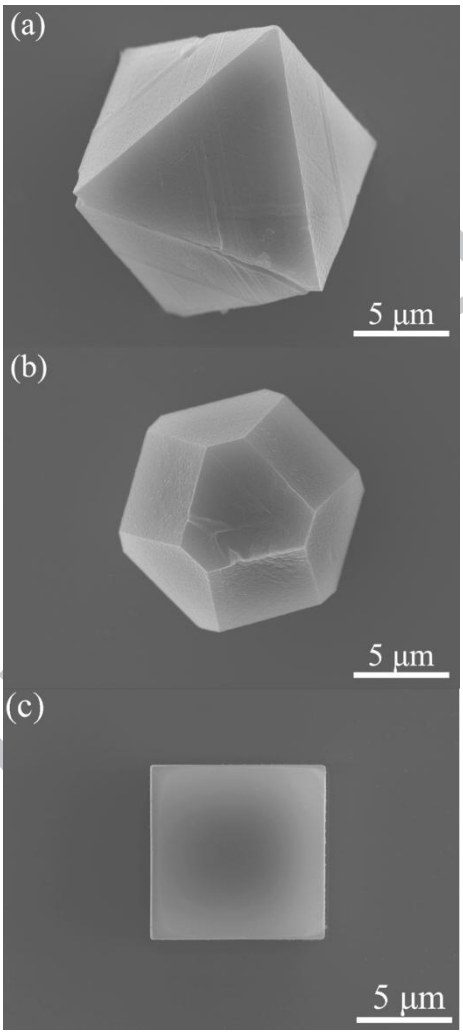

Figure 1. SEM images of octahedral (a), tetrakaidecahedral (b) and cubic (c) HKUST-1 prepared with different LDH/BTC molar ratio (a: 0; b: 0.03; c: 0.05)

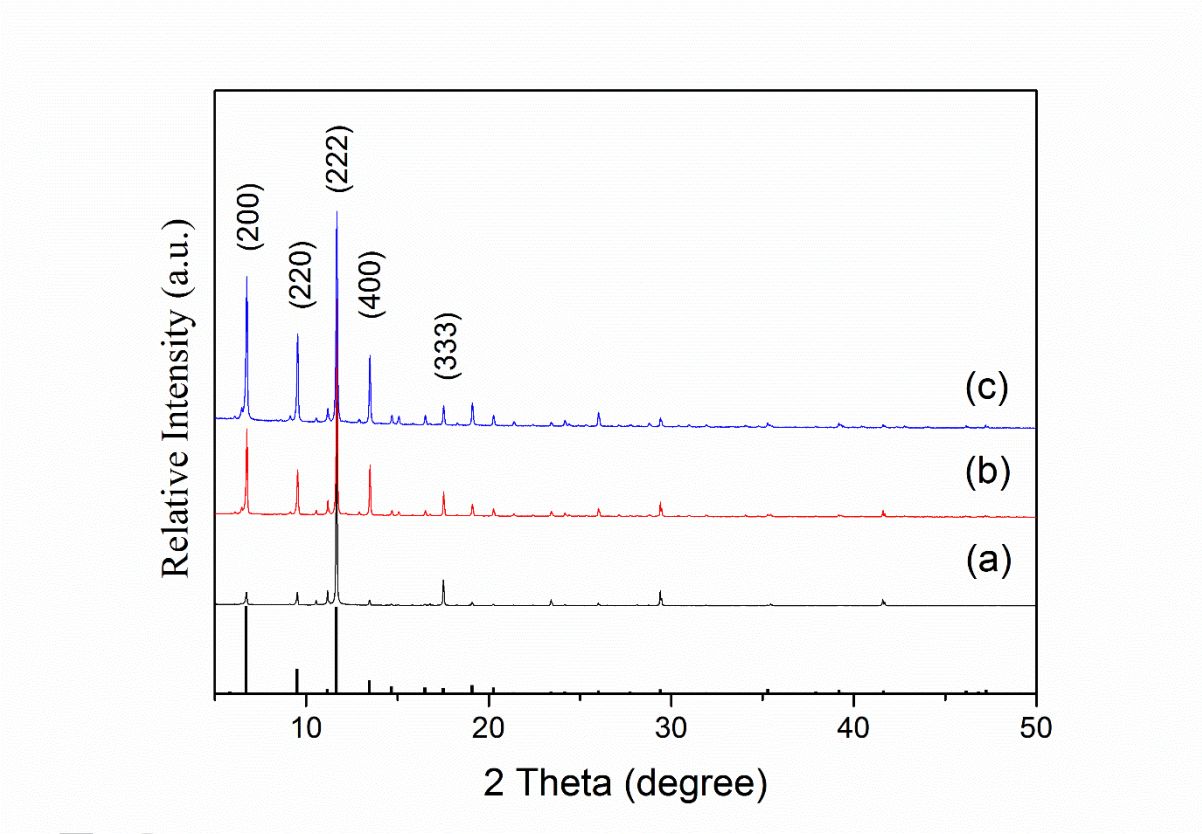

Figure 2. XRD patterns of as-prepared octahedral (a), tetrakaidecahedral (b), cubic (c) and simulated HKUST-1

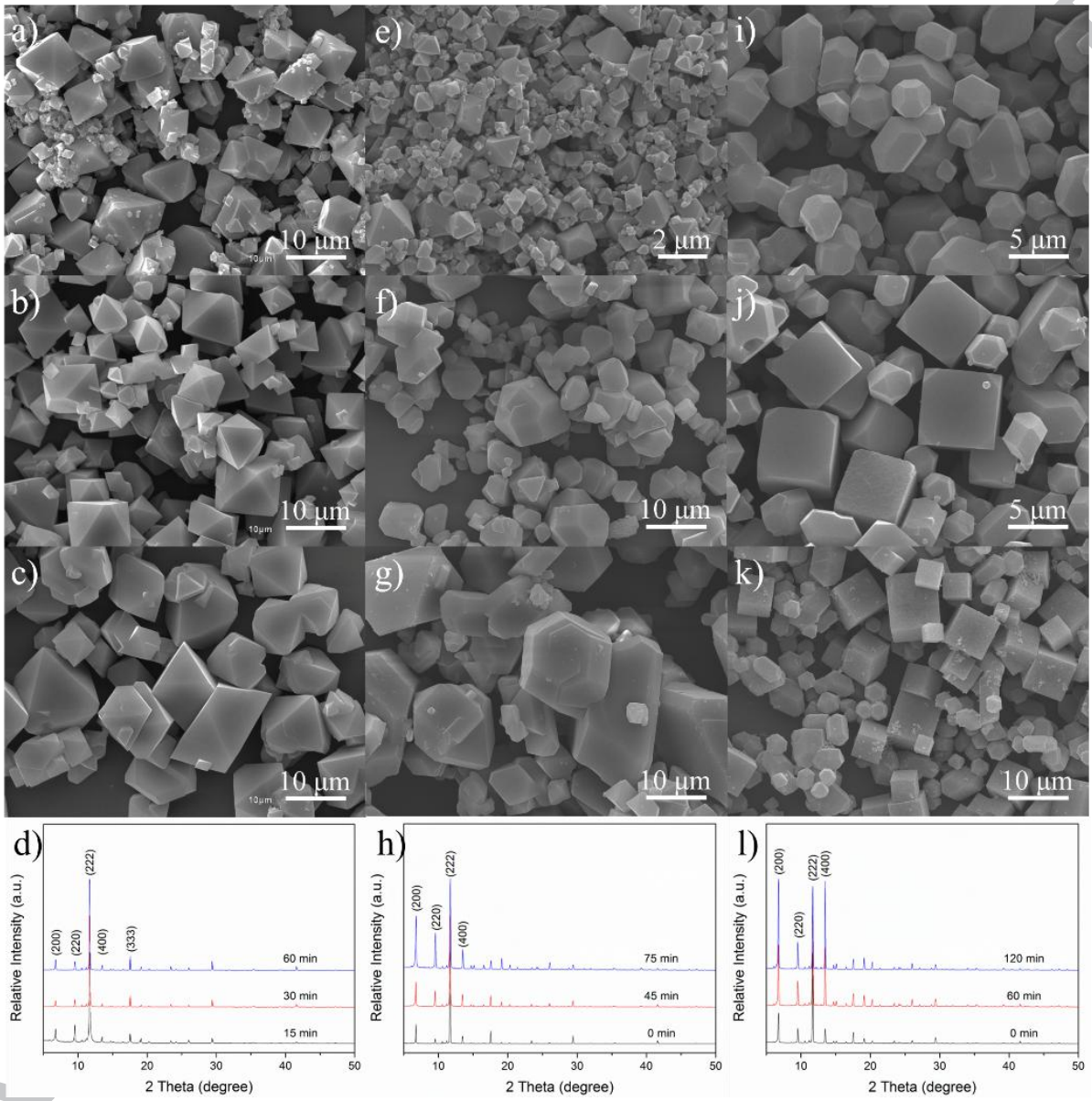

Figure 3. Morphological evolution of octahedral (a, b, c, d), tetrakaidecahedral (e, f, g, h), cubic (i, g, k, l) HKUST-1 synthesised with different heating duration time of 0 (a, e, i), 30 (b), 45(f), 60 (j, c), 75 (g) and 120min (k); Corresponding XRD pattern were shown at the bottle of SEM image.

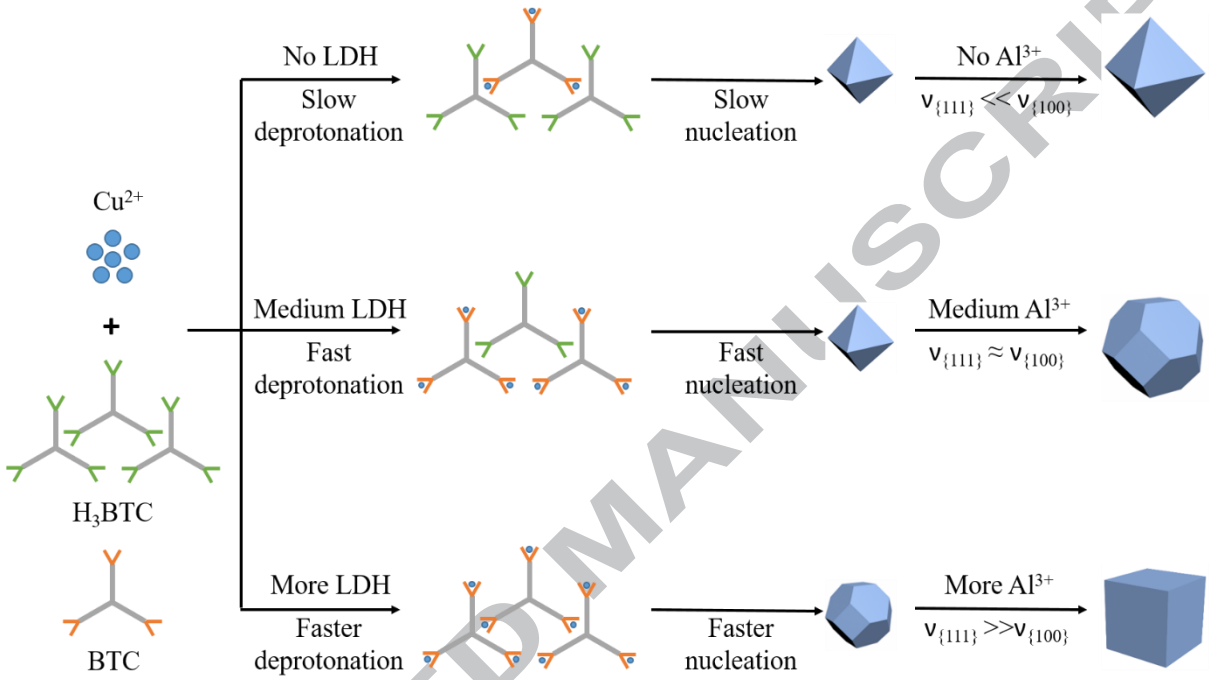

Scheme 2. Schematic illustrations of the mechanism for the orientated growth of HKUST-1 by LDH modulation.

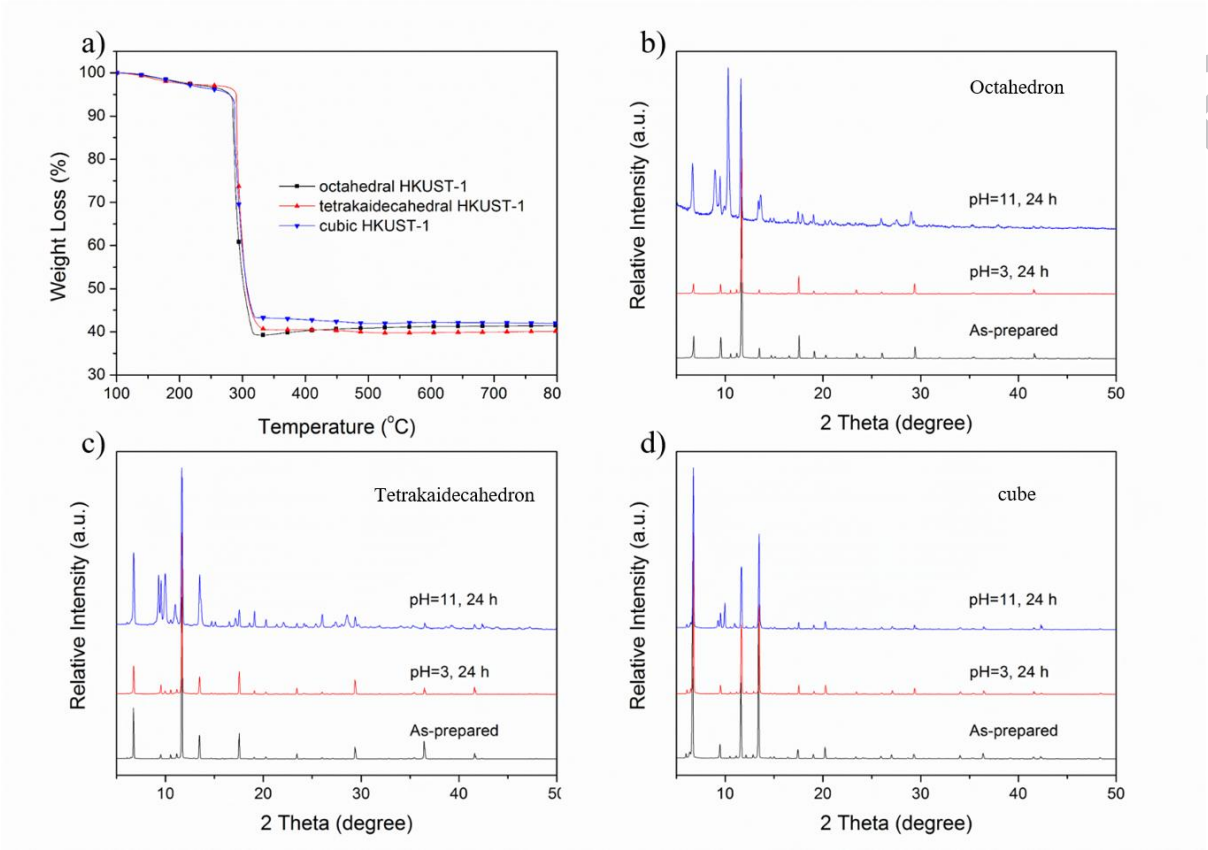

Figure 4 TGA curves of HKUST-1 (a) and XRD patterns of octahedral (b), tetrakaidecahedral (c), cubic (d) HKUST-1 under different conditions.

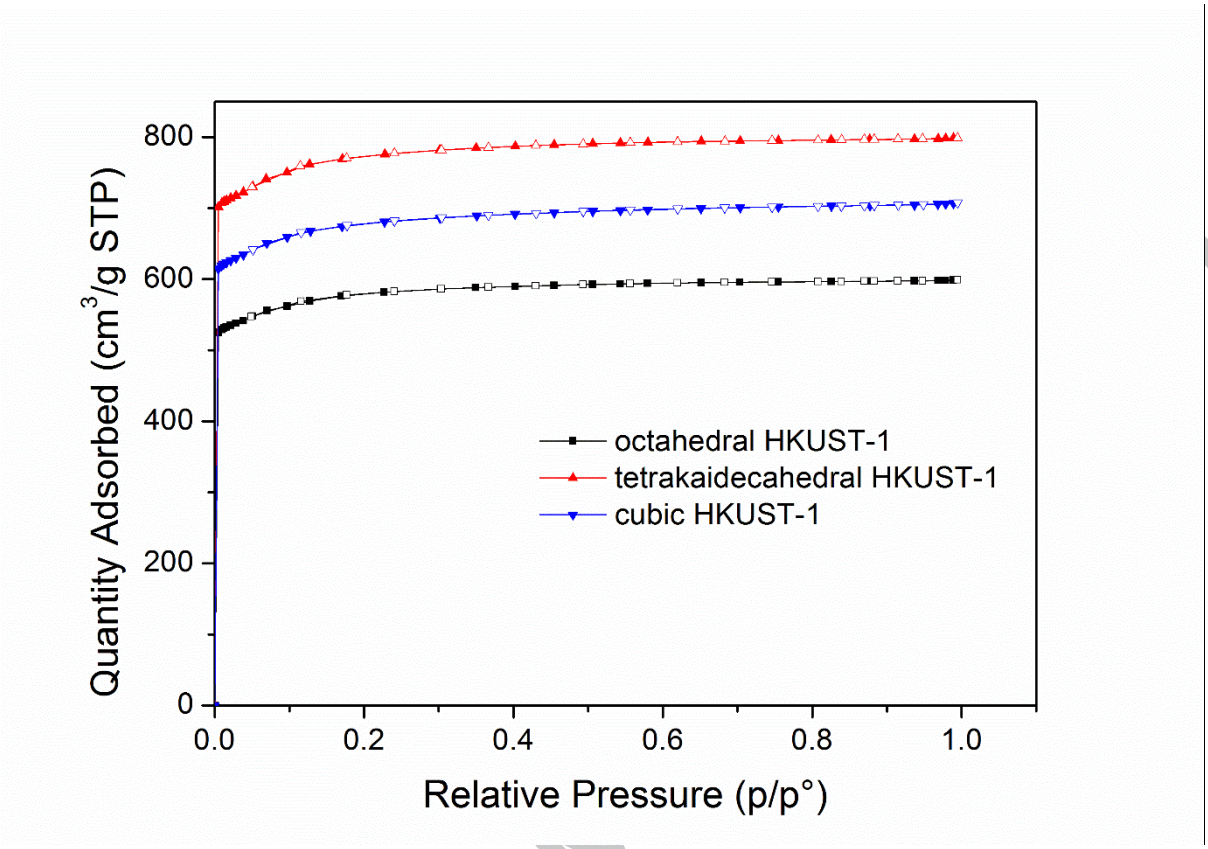

Figure 5. N_2 sorption isotherms at 77K for HKUST-1 with different morphologies

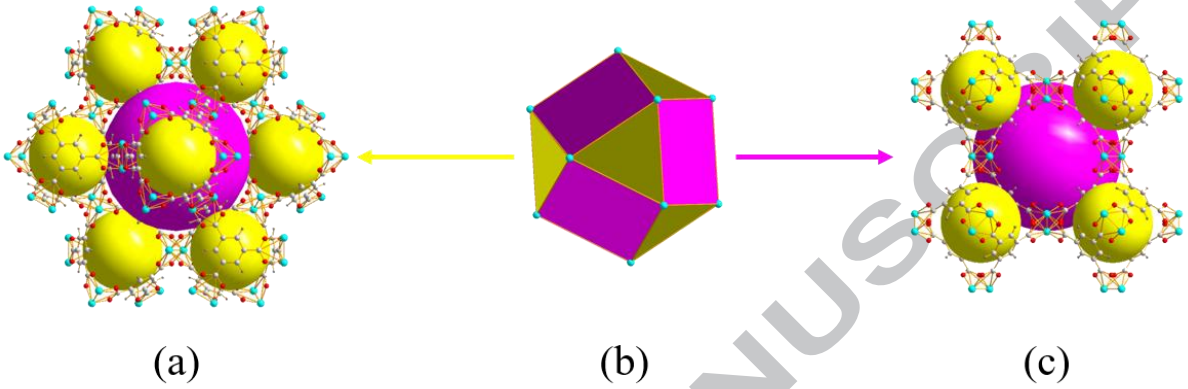

Figure 6. Unit cells of HKUST-1 projected along <111> (a) and <100> (c); (b) a standard growth unit with 8 triangle window (yellow) for {111} facets and 6 square window (purple) for {100} facets

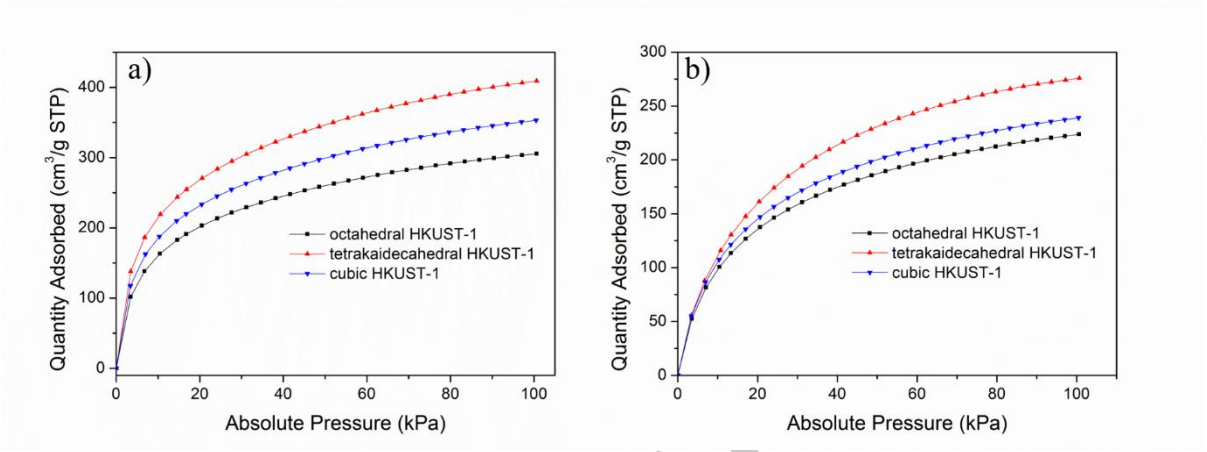

Figure 7. Acetylene adsorption isotherms of HKUST-1 with different morphologies at 273K (a) and 298K (b)

Highlights

- Layered double hydroxide nanosheets were applied as modulator for crystal growth.
- Different orientated growth of HKUST-1 were observed.
- The exposure of <100> facets facilitated the removal of guest molecular.
- Surface area and pore volume of HKUST-1 were enhanced by orientated growth
- Tetrakaidecahedral HKUST-1 exhibited high acetylene uptake at ambient condition.

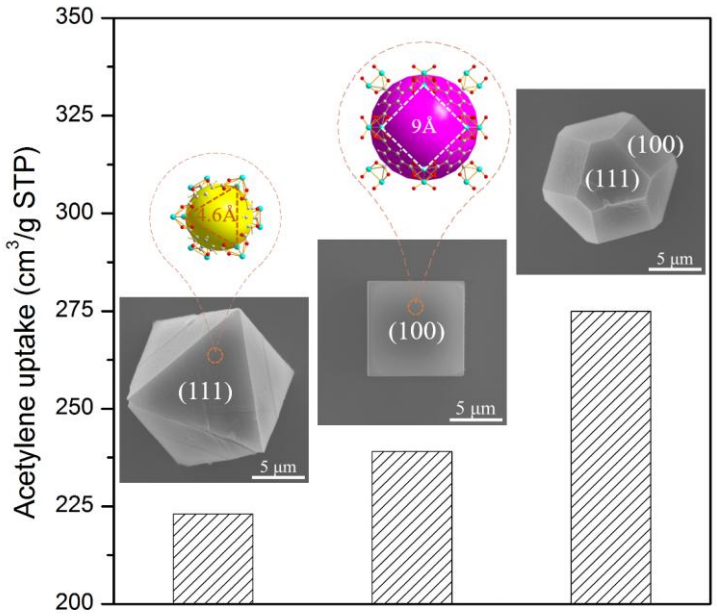

Mg/Al layered double hydroxide (LDH) nanosheets have been applied as modulators to tune the growth orientation of HKUST-1. The derived tetrakaidecahedral HKUST-1 crystals are free of impurity and pore blockage, exhibiting high acetylene uptake at room temperature.